· Article · Advances in Polar Science
doi: 10.13679/j.advps.2019.0024 December 2019 Vol. 30 No. 4: 382-390

Methane increase over the Barents and Kara seas after the autumn pycnocline breakdown: satellite observations

Leonid YURGANOV[1*], Frank MULLER-KARGER[2] & Ira LEIFER[3]

[1] University of Maryland Baltimore County (ret), Baltimore, MD, USA;
[2] University of Southern Florida, St. Petersburg, FL, USA;
[3] Bubbleology Research International, Inc., Solvang, CA, USA

Received 1 July 2019; accepted 31 October 2019; published online 9 December 2019

Abstract Seven operative thermal infrared (TIR) spectrometers launched at sun-synchronous polar orbits supply huge amounts of information about Arctic methane (CH_4) year-round, day and night. TIR data are unique for estimating CH_4 emissions from a warming Arctic, both terrestrial and marine. This report is based on publicly available CH_4 concentrations retrieved by NOAA and NASA from spectra of TIR radiation delivered by EU IASI and US AIRS sounders. Data were filtered for high thermal contrast in the troposphere. Validation versus aircraft measurements at three US continental sites reveal a reduced, but still significant sensitivity to CH_4 anomalies in the troposphere below 4 km of altitude. The focus area is the Barents and Kara seas (BKS). BKS is impacted with warm Atlantic water and mostly free of sea ice. It is a shelf area with vast deposits of oil and natural gas (~90% CH_4), as well as methane hydrates and submarine permafrost. Although in summer AIRS and IASI observe no significant difference in CH_4 between BKS and N. Atlantic, a strong, monthly positive CH_4 spatial anomaly of up to 30 ppb occurs during late autumn–winter. One of explanations of this increase is a fall/winter pycnocline breakdown after a period of blocked mixing caused by a stable density seawater stratification in summer: enhanced mixing lets CH_4 to reach the sea surface and atmosphere.

Keywords **satellite data, greenhouse gases, Arctic**

Citation: Yurganov L, Muller-Karger F, Leifer I. Methane increase over the Barents and Kara seas after the autumn pycnocline breakdown: satellite observations. Adv Polar Sci, 2019, 30(4): 382-390, doi: 10.13679/j.advps.2019.0024

1 Introduction

The Arctic has experienced the fastest warming on Earth over recent decades, termed Arctic amplification, with the Arctic Ocean warming at nearly double the rate of the world's oceans (Hoegh-Guldberg and Bruno, 2010). Due to Arctic warming, there is concern that the vast stores of the important greenhouse gas methane (CH_4) in hydrates, permafrost, and other vulnerable reservoirs can be released to the atmosphere. The radiative impact of CH_4 is second after carbon dioxide on century timescales, and larger on decadal timescales (Solomon et al., 2007). Warm Atlantic currents make the Barents and Kara seas (BKS) climatically important with respect to instability of seabed CH_4 due to the input of warming seawater. The Barents Sea is a shallow-shelf sea (average depth 230 m) with depressions to 400 m. It currently is close to ice-free year-round (Onarheim and Årthun, 2017). The Kara Sea is even shallower (average depth 100 m) and ice-free in summer. The BKS has extensive proven oil and natural gas deposits, the latter of which are primarily CH_4 (Shipilov and Murzin, 2002). Although rather limited, existing data show these reservoirs drive CH_4 seepage into the water column (Chand et al., 2014; Platt et al., 2018). At depths greater than 250 m CH_4 forms hydrates that are stable in the cold BKS deep waters (~1 ℃). Additional seabed CH_4 is sequestered in the

* Corresponding author, E-mail: leonid.yurganov@gmail.com

Kara Sea and the South Barents Sea as submarine permafrost (Osterkamp, 2010). Warming seabed water may destabilize submarine permafrost and hydrates, although specific mechanisms and timescales are uncertain.

Most seep bubble CH_4 dissolves in process of ebullition in deep water where methanotrophic bacteria oxidize it on weeks' to years' timescales (Reeburgh, 2007). Only a small fraction of the seep bubble methane directly reaches the air. The seasonal summer pycnocline prevents vertical turbulent diffusion of methane, with concentrations near the seafloor that may be extremely high (Gentz et al., 2014). They studied dissolved CH_4 concentrations to the West of Prins Karls Forland (Svalbard) in August 2010 (not in winter) and found that CH_4 bubble plumes dissolved below the pycnocline and were not vertically mixing to the upper water column. They suggested that during winter in high latitudes after the summer stratification breaks down, vertical transport of CH_4 from the bottom layer is not limited anymore, and CH_4 can reach the sea surface. The most comprehensive CH_4 measurements at the seafloor and in the atmosphere in the region were collected to the West of Svalbard in June–July, 2014, by Myhre et al. (2016). They found that summer CH_4 release from seabed sediments substantially increases CH_4 concentrations above the seafloor with a sharp decrease above the pycnocline. They suggest that dissolved methane captured below the pycnocline may only be released to the atmosphere when physical processes remove the pycnocline as a dynamic barrier. Mau et al. (2017) field measurements between Svalbard and Bear Island in August–September, 2015, also demonstrated the pycnocline as a barrier for CH_4. All three investigations came to a conclusion on insignificant methane flux in summer-early autumn around Svalbard and between Svalbard and Bear Island. Meanwhile, as it is well known (Rudels, 1993), during winter in high latitudes convective mixing extends to the seafloor. Currently, this seasonality of potential CH_4 pathways has not been considered in CH_4 budgets (Fisher et al., 2011; AMAP, 2015). To our best knowledge, direct measurements of CH_4 flux in winter have not been published for the BKS to date. Summertime CH_4 emission density near Svalbard was estimated by Myhre et al. (2016) as 0.04 $nmol \cdot m^{-2} \cdot s^{-1}$. Formal extrapolation onto the whole year and total area of BKS (2.317×10^9 km^2) results in 0.047 Tg $CH_4 \cdot a^{-1}$, i.e. negligible flux.

Shakhova et al. (2010) investigated summer and winter methane flux from the East Siberian Arctic Shelf (ESAS) encompassing the Laptev, East Siberian seas, and Russian part of the Chuckchi Sea. More than 5000 at-sea measurements of dissolved methane have been collected. Greater than 80% of ESAS bottom waters and greater than 50% of surface waters were supersaturated with methane regarding to the atmosphere. In summer diffusive and ebullition fluxes were estimated, respectively, as 1.24 Tg CH_4 and 1.68 Tg CH_4 (total summer 2.92 Tg CH_4), in winter 3.23 Tg CH_4 and 4.49 Tg CH_4 (total winter 7.72 Tg CH_4), totally 10.64 Tg $CH_4 \cdot a^{-1}$. An assessment by Berchet et al. (2016) based on surface NOAA network and inverse modeling is significantly lower: 0.5–4.3 Tg $CH_4 \cdot a^{-1}$.

Satellite observations are extremely useful for characterization of Arctic CH_4, especially over open sea, due to their continuous and global data record. Thermal infrared (TIR) CH_4 data are available globally, day and night, whereas SWIR CH_4 instruments are ineffective in the Arctic due to low or no sunlight, low reflectivity from water and ice, and long atmospheric optical path (Leifer et al., 2012). TIR orbital sensors include AIRS/Aqua, IASI/MetOp-A, B, C, CrIS/NPP, CrIS/NOAA-20, and GOSAT/TANSO-TIR (see a list of abbreviations at the end of the article). Example current SWIR sensors are TROPOMI and GOSAT-SWIR.

CH_4 retrievals for AIRS and IASI are publicly available (see links in Section 2.1). Yurganov et al. (2016) suggested a filtering technique for the Arctic data and presented data on seasonal, spacial and interannual variability of methane in the layer below 4 km. They concluded, "Seasonal increase in methane has been observed since late October–early November. This can be associated with the beginning of vertical convection in the ocean, caused by the cooling of the surface layers and the simultaneous increase in temperature of the underlying water layers. Bottom layers saturated with methane are brought to the surface" (translated from Russian). Preliminarily, Yurganov et al. (2016) assessed the annual emission of methane from the Arctic Ocean in 2010–2014 as ~2/3 of land emission to the North from 60°N. Arctic terrestrial emission is now estimated as 20–30 $Tg \cdot a^{-1}$ (AMAP, 2015). Therefore, total marine CH_4 flux from the Arctic can be expected in the range 15–20 Tg $CH_4 \cdot a^{-1}$ (without the Sea of Okhotsk). The most recent analysis of available measurements of the global methane flux from oceans (Weber at al., 2019) by training machine-learning models gave much lower oceanic flux (6–12 Tg $CH_4 \cdot a^{-1}$). However, their conclusion that very shallow coastal waters contribute around 50% of the total methane emissions from the ocean agrees with our data for the Arctic (see below, Section 3).

Here we show that CH_4 spatial anomaly (SA) over BKS is seasonally growing together with the Mixed Layer Depth (MLD). Therefore, an increase of emission in winter, predicted by Gentz et al. (2013) and Myhre et al. (2016) agrees with remote sensing data and seasonal cycle of MLD. However, this agreement does not exclude other explanations of the effect and a confirmation of a significant wintertime flux from Arctic seas by direct measurements is necessary. After that it may be included into the methane budget.

2 Methods

2.1 Satellite instruments, data, and retrieval techniques

The nadir cross-track scanning diffraction grating spectrometer,

AIRS/Aqua, was launched in May 2002 (Xiong et al., 2008). CH_4 profiles and surface skin temperature (*SST*) are retrieved for a 3×3 matrix of 9 circular 13.5-km diameter pixels. Version 6 of the retrieval algorithm (Susskind et al., 2012) and data (AIRS3STM.006, Aqua L3 Monthly Standard Physical Retrieval, AIRS-only) are available from https://disc.gsfc.nasa.gov/datasets/, since 2002.

The IASI/MetOp-A is a cross-track-scanning Michelson interferometer that measures spectra of outgoing long wave radiation with an apodized resolution of 0.5 cm^{-1} at the ν4 CH_4 band near 7.65 μm wavelength (Razavi et al., 2009). The MetOp-A satellite, operated by EUMETSAT, was launched in 2006. Like AIRS, IASI has a 2200-km swath with a scan swath angle of ±48.3°. The IASI retrieval algorithm NUCAPS was built at NOAA/NESDIS to emulate the AIRS Version 5 code and has been in operation since 2008 (Maddy et al., 2009). Level 2 data for 2×2 matrices of 4 circular, 12-km diameter pixels are available from the NOAA's CLASS site https://www.avl.class.noaa.gov/saa/products/.

Both satellites are currently operative and have sun-synchronous polar orbits: a geometry that favors polar coverage. Aqua and MetOp-A cross the equator at approximately 01:30 and 13:30; 09:30 and 21:30 local time, respectively. Retrieval algorithms for these two instruments are similar but not identical. For both, CH_4 retrieval accuracy depends on the accuracy of temperature, humidity, and surface emissivity retrievals. The latter is highly important for land, but unimportant for the water surface. Pixel matrices combined with microwave radiometer field of view allow retrieval of CH_4 profiles for cloud-free and partially-clouded pixels (Susskind et al., 2003). The significantly higher spectral resolution of IASI (0.5 cm^{-1}) compared to that of AIRS (~1.5 cm^{-1}) is a reason for giving preference to IASI data.

Data over the North Atlantic and BKS with sufficiently high vertical thermal contrast (*ThC*) were analyzed. *ThC* is defined as the temperature difference between *SST* and at the 4 km altitude; a criterion $ThC > 10$ ℃ was suggested by Yurganov et al. (2016).

As it will be presented below, Arctic CH_4 data for these two instruments and retrieval techniques are in agreement. At the same time, it should be noted that both retrieval techniques were developed primarily for weather prediction purposes and global conditions. Atmospheric gases data from them are still qualified as "research" products. Arctic environment is very specific: there are seasonal changes in sea ice area and thickness, winter temperature inversions are often, the network of "ground truth" information is sparse, etc. This paper should be considered as a pilot one; a specific retrieval procedure should be developed for Arctic with inclusion radiation data from as many instruments as possible and the most comprehensive atmospheric state information (temperature and humidity profiles, surface emissivity, etc).

A comprehensive analysis of NUCAPS and AIRS v6 uncertainties for specific Arctic conditions requires the retrieval code. It is unavailable for public: we used just results of the retrievals. A measure of uncertainty in this situation is standard deviation of individual retrievals. It is between 20 and 30 ppb over BKS. Normally there are ~30 points per 0.5°×0.5° grid cell per one month or 120 points per 1°×1° grid cell per month and ~2000 points for box #8 per month. Therefore, standard deviations of the monthly means are: 5–6 ppb for 0.5°×0.5° grid cell and ~0.7 ppb for box #8. More information about accuracy of the data can be found in a response to a reviewer of a discussion paper by Leifer et al. (2019).

2.2 CH_4 retrieval validation

For comparison we used CH_4 mixing ratios near the surface that were sampled weekly at coastal stations in Iceland (ICE) and Svalbard, Norway (ZEP). Validation versus aircraft profiles of CH_4 have been implemented at three US sites for entire period of 2003–2018: Trinidad Head (THD) in Northern California, Southern Great Plains (SGP) in Oklahoma and near Charleston (SCA) in South Carolina. The surface and aircraft samples were analyzed at the NOAA/GMD/ESRL laboratory in Boulder, Colorado, surface data are available at ftp://aftp.cmdl.noaa.gov/data/trace_gases/ch4/flask/surface/; aircraft data are kindly supplied by Colm Sweeney (NOAA/GMD/ESRL).

AIRS- and IASI-derived CH_4 concentrations and anomalies below 4 km altitude (termed Low Troposphere, LT) and above 4 km (Mid-upper Troposphere, MUT) were validated with airborne CH_4 measurements at three sites in the USA (Figure 1). For MUT, satellite and airborne measurements agree better than for LT with slopes close to 1. For the lower troposphere, data show good correlation but with slopes close to 0.5. We propose that this slope, calculated from a least squares linear regression analysis (Table 1 calculated by MATLAB) provides an empirical sensitivity (*S*). *S* was derived for both the LT and MUT (between 4 and 8 km of altitude):

$$S = \Delta C_{ret} / \Delta C_{real}, \quad (1)$$

where C_{ret} and C_{real} are the retrieved CH_4 and aircraft, altitude-averaged, CH_4 concentrations, respectively. ΔC is the anomaly of concentration, spatial (SA) or temporal (TA).

The validation (Figure 1 and Table 1) shows a common feature for both instruments: MUT slopes are ~1.0 whereas LT slopes are between 0.3 and 0.5. Correlation coefficients (R^2) range from 0.75 to 0.92. The higher sensitivity *S* above 4 km relative to 0–4 km is probably due to a greater thermal contrast in MUT compared to LT.

One should discriminate between the anomaly accuracy and the concentration accuracy. For MUT our validation effort shows a good TA accuracy and a moderate bias in concentration (Table 1 calculated by MATLAB). For LT a significant

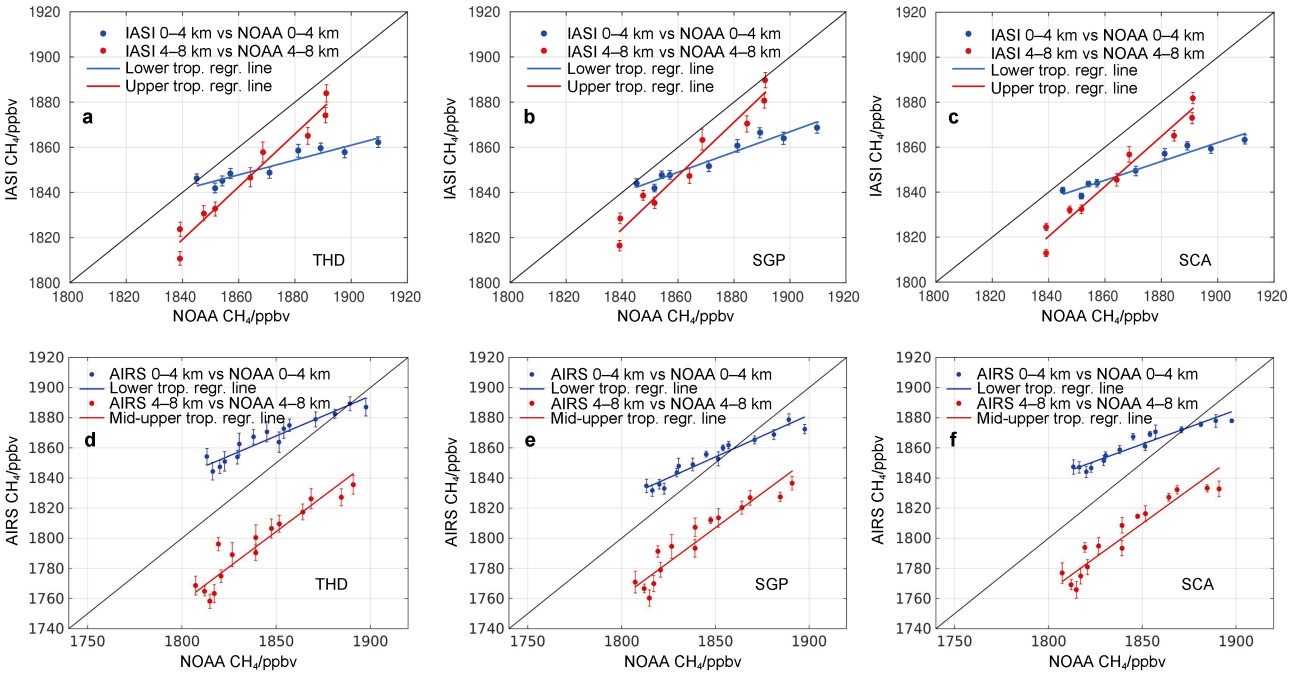

Figure 1 April–September IASI CH_4 data for LT (blue) and MUT (red) compared with concentrations measured from NOAA aircrafts at 3 sites in USA: Trinidad Height, CA (THD), Southern Great Plain, OK (SGP), and Charleston, SC (SCA) (**a**–**c**). The same, but for AIRS. Error bars correspond to $STD/(N-1)^{1/2}$, where N is number of points included into the mean (**d**–**f**).

underestimation in concentration up to 40 ppb and a 50% underestimation of TA may occur. The LT TA error, however, is persistent for all three sites and both instruments; this systematic error should be just taken into account at the analysis stage. A great advantage of the LT data is a proximity of the atmospheric domain to the surface sources. MUT is characterized much higher winds that mix the atmosphere effectively. Further details of the satellite CH_4 validation and accuracy can be found in Yurganov et al. (2016) and in a response to a reviewer of a discussion paper by Leifer et al. (2019).

Table 1 Parameters of linear regression for three NOAA/ESRL validation sites

NOAA code and altitudes	Slope	Intercept/ppb	LCB	UCB	R^2	Bias/%
			IASI			
THD, 0–4 km	0.33	1237.53	0.23	0.43	0.77	−1.12
THD, 4–8 km	1.17	−330.44	0.96	1.38	0.92	−0.9
SGP, 0–4 km	0.45	1015.71	0.35	0.55	0.92	−0.97
SGP, 4–8 km	1.18	−353.83	0.95	1.42	0.92	−0.63
SCA, 0–4 km	0.42	1067.63	0.33	0.51	0.92	−1.19
SCA, 4–8 km	1.11	−225.21	0.92	1.3	0.92	−0.91
			AIRS			
THD, 0–4 km	0.49	958.34	0.38	0.6	0.77	1.14
THD, 4–8 km	0.93	89.94	0.71	1.14	0.75	−2.3
SGP, 0–4 km	0.51	900.87	0.41	0.62	0.8	0.3
SGP, 4–8 km	0.91	116.2	0.71	1.12	0.77	−2.27
SCA, 0–4 km	0.45	1037.79	0.36	0.53	0.82	0.83
SCA, 4–8 km	0.92	103.2	0.75	1.1	0.83	−2.17

Notes: LCB and UCB are lower and upper confidence bounds for slope at 95% confidence calculated according to Chatterjee and Hadi (1986). R is correlation coefficient.

2.3 Ocean mixed layer depth calculations

MLD was estimated from the ECCO2 global model. ECCO2 is a Phase II of the High-Resolution Global–Ocean and Sea–Ice Data Synthesis, sponsored by the NASA (Wunsch et al., 2009). The model has spatial resolution of 0.25° with 50 vertical levels. Daily average MLD was estimated as the depth at which the potential density relative to the surface is larger than surface density ρ by using the $\Delta\rho$ =0.8 ℃ × α criterion, where ρ is the density and α is the seawater thermal expansion coefficient at the surface (Kara et al., 2003). Comparisons with field measurements confirm that model accuracy is better than 20 m (Kara et al., 2003).

3 Results

Monthly mean maps of IASI LT CH_4 (Figure 2) demonstrate a surprisingly spatially homogeneous CH_4 distribution over the entire Arctic Ocean between May and September. This is in contrast to the heterogeneity observed beginning in October where strongly enhanced methane is observed over various Arctic seas.

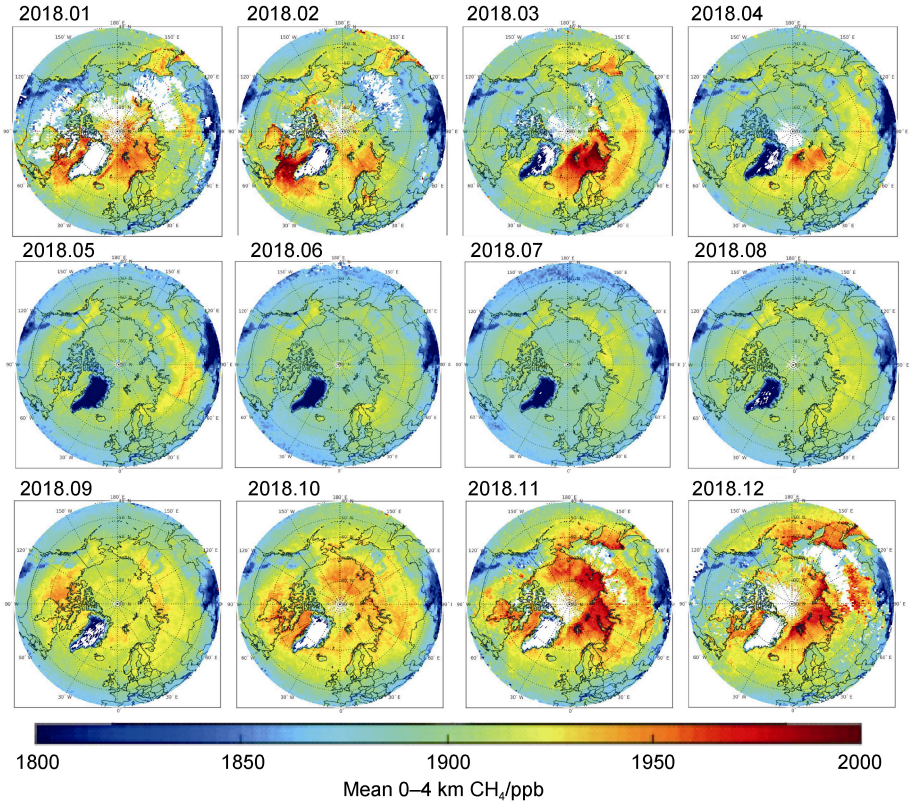

Figure 2 Monthly mean IASI LT CH_4 concentrations in 2018.

Monthly mean BKS maps for June and December (Figure 3, a–d) for both IASI and AIRS show similar patterns and trends, with IASI showing structures in CH_4 at higher fidelity and higher enhancement—likely the result of higher spectral resolution. Seasonal variation of LT CH_4 from IASI was analyzed for selected boxes in the BKS, designated 1 to 7 on a path from Iceland to the North Kara Sea (Figure 3b). IASI found increased methane in narrow bands along coasts of Norway, Novaya Zemlya, and Svalbard in December. These local coastal enhancements need further evaluation and comparison with *in situ* data to avoid misinterpretation; they are not analyzed further.

The annual cycle amplitudes (from minimum to maximum, a kind of TA) for selected boxes (Figure 3e) increases gradually and persistently from box #1 (~25 ppb) to box #7 (~55 ppb), i.e., a factor of 2. These remote sensing data are in a qualitative agreement with *in situ* NOAA flask measurements at the Svalbard (Zeppelin, ZEP) observatory and at the Iceland NOAA site (ICE), thick lines at Figure 3e (an offset of 18 ppb is subtracted from all surface data for comparability). The cycle amplitude of measured surface methane in Svalbard is ~30% higher than for Iceland.

Box #8 to the SW from Svalbard is adjacent to the area investigated by Gentz et al. (2014), Figure 3b. This area is at the edge of the continental shelf and also is known for numerous seabed seeps mapped by ships. We calculated the CH_4 seasonal SA as the differences between IASI data for box #8 and the average of boxes #1 and #2 (the Barents Sea Opening), then we compared them with *in situ* SA between

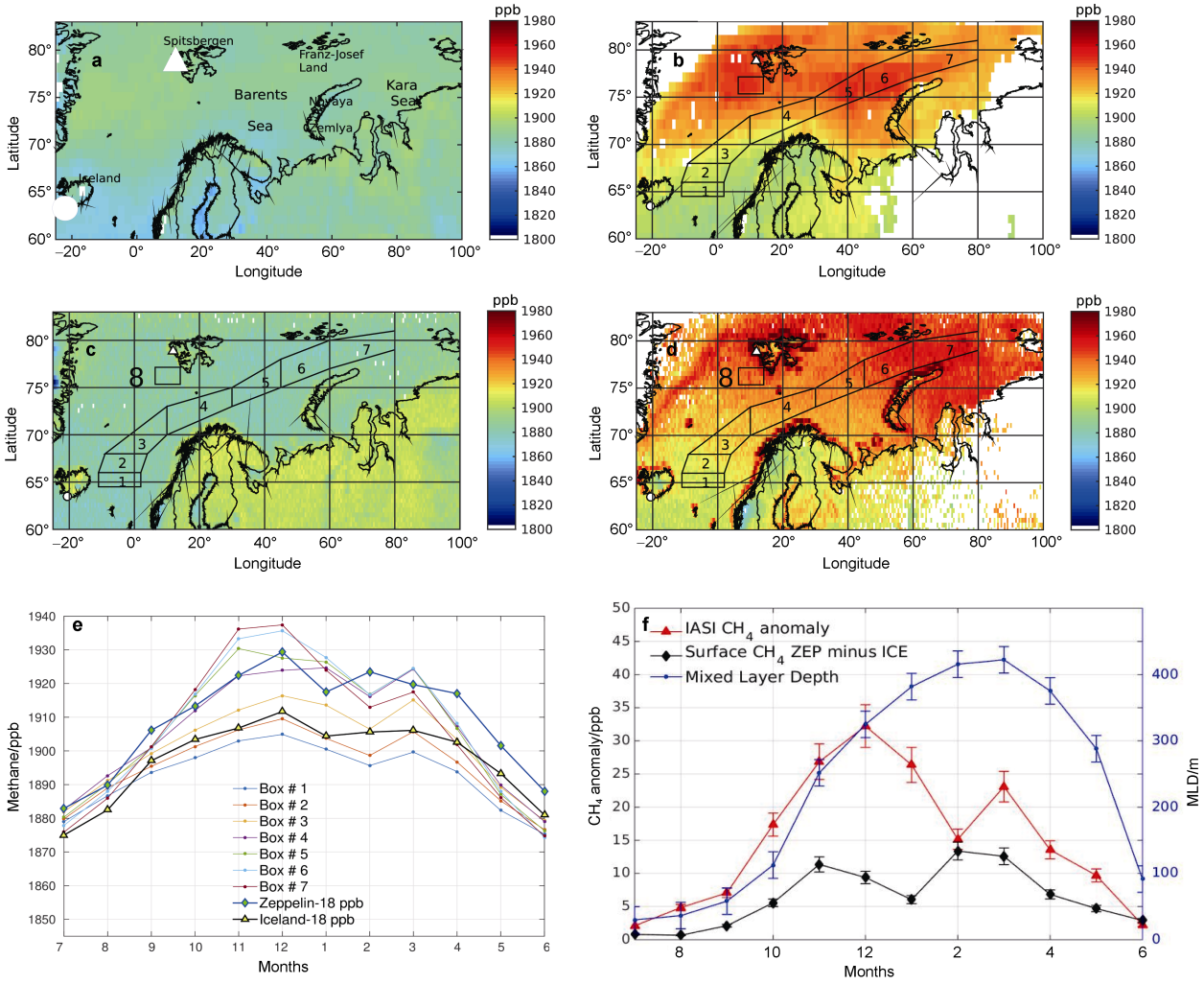

Figure 3 Mean LT CH_4 concentrations measured by AIRS for 2013–2015 in June and December, respectively (**a**–**b**); mean LT CH_4 concentrations measured by IASI for 2014–2018 in June and December, respectively (**c**–**d**). Locations of surface stations ICE and ZEP are shown by a circle and a triangle, respectively. Monthly mean LT concentrations measured by IASI and averaged over 2014–2018 for boxes shown on the maps above. Surface concentrations has been moved downward by 18 ppb for comparability (**e**). Red line is a difference between concentrations for the box #8 and combined boxes #1–#2 (**f**). Black line is for a difference between surface CH_4 at ZEP and ICE. Blue line is for the box #8 seawater MLD. All three lines are 2014–2016 averages. Error bars correspond to $STD/\ (N-1)^{1/2}$.

ZEP and ICE (Figure 3f): both curves have two maxima, in November–December and in March, but amplitudes of seasonal cycles were different; that may be explained by different techniques and/or different atmospherics domains.

Patches of increased methane in winter can be explained by the density stratification breakdown allowing CH_4 from deeper water including sources to reach the atmosphere. To validate this hypotheses we extracted MLD for the box #8 located to the SW from Svalbard (Figure 3f, blue curve). The shape of the MLD cycle is very similar to the shape of methane SA for the same location. The maximum mixing depth up to 400 m is sufficient to transport methane from the seabed to the surface.

A good agreement between methane monthly anomalies and MLD is observed also for the total period of AIRS measurements (Figure 4). Note an agreement between monthly SA measured by AIRS and IASI during their common period of measurements (2010–2016). On the same graph monthly mean *SST* for the box #8 are plotted. The variations of *SST* are found to be out of phase with MLT, as expected: in autumn, after breakdown of stratification, cooler and CH_4-richer seawater replaces the summer warmer and fresher seawater.

4 Discussion

A combination of two conditions are necessary and sufficient for a significant flux of CH_4 from sea to air. First, there should be seabed or seawater CH_4 sources either in the region or an upcurrent region. Second, there should be an effective transport of CH_4 from the source to the surface

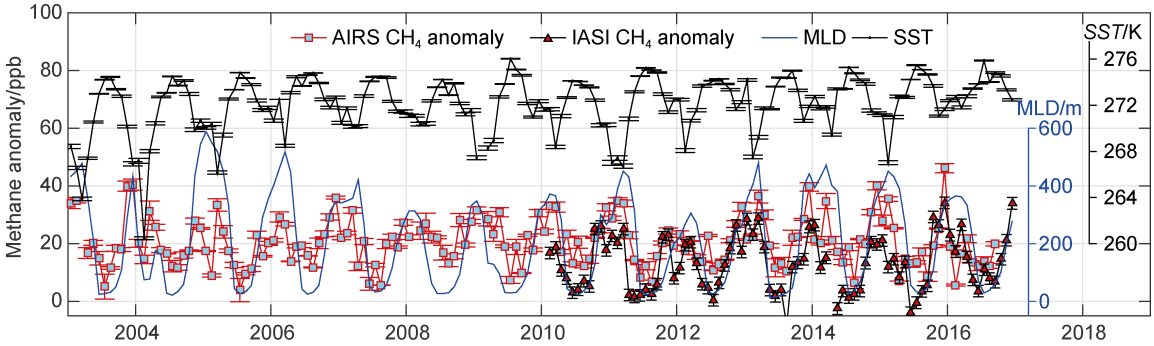

Figure 4 CH_4 monthly anomalies (LT concentration differences between box #8 and combined boxes #1 and #2) according to AIRS and IASI measurements. Blue line is smoothed daily MLD calculated for the box #8 (accuracy ± 20 m). Also shown are monthly mean *SST* for the box #8. Error bars correspond to $STD/(N-1)^{1/2}$.

seawater layer. A significant emission of CH_4 from the seafloor to deep water layers around Svalbard and along a path Svalbard–Bear Isl. has been documented (see the Introduction). All these results show negligible CH_4 flux and are obtained in summer months or in September, i.e., before a breakdown of the pycnocline. Gentz et al. (2014) and Myhre et al. (2016) predict a much higher methane flux in winter, when a transport by an intense turbulent diffusion and convection occurs.

The BKS is known for extensive methane seeps explained by oil and natural gas deposits (Shipilov and Murzin, 2002). Remote sensing data on CH_4 in the lower troposphere over the winter Arctic Ocean presented in this article confirm predictions of Gentz et al. (2014) and Myhre et al. (2016) and evidence in favor of a significant emission of CH_4 from BKS. Moreover, satellites allow one not only to assume a significant winter methane flux, but also to give an idea on areas where this emission may occur, as well as about its annual cycle. Specifically, maximum CH_4 SA for BKS is observed in November–December with a secondary maximum in March. Noteworthy is that the pycnocline is not a barrier for bubbles: this kind of CH_4 transport should be effective year-round, it's a barrier to turbulent transport of dissolved CH_4. Negligible summer CH_4 suggests direct ebullition transport to the atmosphere is not sufficient to create significant anomalies on monthly bases. Numerous *in situ* spikes observed by Leifer et al. (2019) at the Barents Sea in August–September, 2013, probably are explained by local seeps.

IASI data (Figure 3d) (Yurganov and Leifer, 2016a) show increased CH_4 SA in narrow bands along the coasts of Norway, Novaya Zemlya, and Svalbard, but not other coasts. Unfortunately, as Leifer et al. (2019) noted, there may be problems in the retrieval algorithm (NUCAPS) for partially land/sea pixel retrievals. This raises the potential for biases in coastal results and argues for the need for improved retrieval technique.

Other vast areas of strong CH_4 SA include Baffin Bay, seas along the East Siberia coast (Figure 2), the Bering Sea and the Sea of Okhotsk (Yurganov and Leifer, 2016b). Methane hydrates exist beneath the sea bottom near cold seeps NE off the Sakhalin in the Sea of Okhotsk (Shoji et al., 2005). This sea, like BKS (Shipilov and Murzin, 2002), is a target area of gas hydrates exploration. One may speculate that methane hydrates of geologic origin, including direct seeps and methane hydrates at BKS and Sea of Okhotsk, is a significant source of CH_4 in the Arctic.

The MLD global maps (Kara et al., 2002) clearly indicate that enhanced vertical mixing to depths of 250 m or deeper occurs in winters of both hemispheres in Northern Atlantic (40°N and above), and in the Southern Ocean (40°S and below). One may expect a significant flux of CH_4 from the Southern Ocean to the atmosphere between June and November, if CH_4 sources present (e.g., microbiological ones, as proposed by Kelley and Jeffrey, 2002).

There are significant regional climate implications of enhanced Arctic winter marine CH_4 emissions which depend on the nature of the source(s). Seeps from extensive hydrocarbon reservoirs at BKS (Shipilov and Murzin, 2002) could lead to formation of methane hydrates of geological origin, submerged permafrost, methane hydrates of biological sources, microbial production in the benthic zone. Satellite data supply little or no information about the nature of the sources. Given that increasing seabed temperatures will lead to increased hydrate dissociation, there are important implications for future emissions. As such, the elucidation of methane hydrate amounts and locations, and vulnerability to warming should be a matter of further research. A valuable feature of satellite data is a possibility to track changes in methane over areas with different sources over a long period of time since 2003.

5 Conclusions

Satellite measurements of CH_4 concentration in the lower 4 km of the troposphere reveal a significant, up to 30 ppb, monthly anomaly referenced to North Atlantic maximized in November–December–January over vast areas of BKS, as well as a part of the Greenland Sea. Satellite observations

show similar, but less pronounced, anomalies in autumn–winter over other Arctic seas (Yurganov et al., 2016; Yurganov and Leifer, 2016a). This CH_4 anomaly may be interpreted as intensification of CH_4 flux induced by turbulent diffusion and/or convection after a breakdown of the summer stratification. After a confirmation of a significant wintertime flux from Arctic seas by direct measurements the marine CH_4 emission may be included into the methane budget.

Abbreviations

AIRS: Atmospheric Infrared Sounder
AMSL: Above Mean Sea Level
BKS: Barents and Kara seas
CLASS: Comprehensive Large Array-data Stewardship System
CrIS: Cross-track Infrared Sounder
ESRL: Earth System Research Laboratory
EUMETSAT: European Organization for the Exploitation of Meteorological Satellites
GMD: Global Monitoring Division
GOSAT: Greenhouse Gases Observing Satellite
GSFC: Goddard Space Flight Center
IASI: Infrared Atmospheric Sounding Interferometer
MLD: Mixed layer depth
NASA: National Aeronautics and Space Administration
NESDIS: National Environmental Satellite, Data, and Information Service
NOAA: National Oceanic and Atmospheric Administration
NPP: National Polar-orbiting Partnership
NUCAPS: NOAA Unique Combined Atmospheric Processing System
ROSES: Research Opportunities in Earth and Space Science
SA: Spatial anomaly
SCIAMACHY: SCanning Imaging Absorption Spectro-Meter for Atmospheric CHartographY
SST: Surface skin temperature
STD: Standard deviation
TA: Temporal anomaly
TROPOMI: TROPOspheric Monitoring Instrument

NOAA/ESRL sampling stations

ICE: Storhofdi, Vestmannaeyjar, Iceland, 63.4ºN, 20.3ºW, 118 m AMSL
SCA: Charleston, South Carolina, USA, 32.77ºN, 79.55ºW, 0 m AMSL
THD: Trinidad Head, California, USA, 41.054ºN, 124.151ºW, 107 m AMSL
SGP: Southern Great Plains, Oklahoma, USA, 36.607ºN, 97.489ºW, 314 m AMSL
ZEP: Zeppelin at Svalbard, Ny-Ålesund, Norway, 78.9ºN, 11.9ºE, 474 m AMSL

Acknowledgments This work was supported by the NASA ROSES-2013 grant: "A.28, The Science of Terra and Aqua: Long-term Satellite Data Fusion Observations of Arctic Ice Cover and Methane as a Climate Change Feedback". Thanks to Colm Sweeney (NOAA/GMD/ ESRL) for providing aircraft CH_4 data.

References

AMAP. 2015. AMAP Assessment 2015: Methane as an Arctic climate forcer. Oslo, 116. http://www.amap.no/documents/doc/AMAP-Assessment-2015-Black-carbon-and-ozone-as-Arctic-climate-forcers/1299.

Berchet A, Bousquet P, Pison I, et al. 2016. Atmospheric constraints on the methane emissions from the East Siberian Shelf. Atmos Chem Phys, 16(6): 4147-4157, doi:10.5194/acp-16-4147-2016.

Chand S, Knies J, Baranwal S, et al. 2014. Structural and stratigraphic controls on subsurface fluid flow at the Veslemøy High, SW Barents Sea. Mar Petrol Geol, 57: 494-508, doi:10.1016/j.marpetgeo.2014.06.004.

Chatterjee S, Hadi A S. 1986. Influential observations, high leverage points, and outliers in linear regression: rejoinder. Statist Sci, 1(3): 415-416, doi:10.1214/ss/1177013630.

Fisher R E, Sriskantharajah S, Lowry D, et al. 2011. Arctic methane sources: isotopic evidence for atmospheric inputs. Geophys Res Lett, 38(21): L21803, doi:10.1029/2011gl049319.

Gentz T, Damm E, von Deimling J S, et al. 2014. A water column study of methane around gas flares located at the West Spitsbergen continental margin. Cont Shelf Res, 72: 107-118, doi:10.1016/j.csr.2013.07.013.

Hoegh-Guldberg O, Bruno J F. 2010. The impact of climate change on the world's marine ecosystems. Science, 328(5985): 1523-1528, doi:10.1126/science.1189930.

Kara A B, Rochford P A, Hurlburt H E. 2003. Mixed layer depth variability over the global ocean. J Geophys Res, 108(C3), doi: 10.1029/2000JC000736.

Kelley C A, Jeffrey W H. 2002. Dissolved methane concentration profiles and air-sea fluxes from 41°S to 27°N. Global Biogeochem Cy, 16(3): 13-1-13-6, doi: 10.1029/2001gb001809.

Leifer I, Chen F R, McClimans T, et al. 2019. Satellite ice extent, sea surface temperature, and atmospheric methane trends in the Barents and Kara seas, The Cryosphere Discuss, Response to Dr. Antonia Gambacorta. https://www.the-cryosphere-discuss.net/tc-2018-237/tc-2018-237-AC3-supplement.pdf.

Leifer I, Tratt D M, Realmuto V J, et al. 2012. Remote sensing atmospheric trace gases with infrared imaging spectroscopy. Eos Trans AGU, 93(50): 525, doi: 10.1029/2012eo500006.

Maddy E S, Barnet C D, Gambacorta A. 2009. A computationally efficient retrieval algorithm for hyperspectral sounders incorporating A priori information. IEEE Geosci Remote S, 6(4): 802-806, doi:10.1109/lgrs.2009.2025780.

Mau S, Römer M, Torres M E, et al. 2017. Widespread methane seepage along the continental margin off Svalbard—from Bjørnøya to Kongsfjorden. Sci Rep, 7: 42997, doi:10.1038/srep42997.

Myhre C L, Ferré B, Platt S M, et al. 2016. Extensive release of methane from Arctic seabed west of Svalbard during summer 2014 does not influence the atmosphere. Geophys Res Lett, 43(9): 4624-4631, doi:10.1002/2016gl068999.

Onarheim I H, Årthun M. 2017. Toward an ice-free Barents Sea. Geophys

Res Lett, 44(16): 8387-8395, doi:10.1002/2017gl074304.

Osterkamp T E. 2010. Subsea Permafrost//Steele J H, Thorpe S A, Turekian K K. Climate and oceans. London UK: Academic Press.

Platt S M, Eckhardt S, Ferré B, et al. 2018. Methane at Svalbard and over the European Arctic ocean. Atmos Chem Phys, 18(23): 17207-17224, doi:10.5194/acp-18-17207-2018.

Razavi A, Clerbaux C, Wespes C, et al. 2009. Characterization of methane retrievals from the IASI space-borne sounder. Atmos Chem Phys, 9(20): 7889-7899, doi: 10.5194/acp-9-7889-2009.

Reeburgh W S. 2007. Oceanic methane biogeochemistry. Chem Rev, 107(2): 486-513, doi:10.1021/cr050362v.

Rudels B. 1993. High latitude ocean convection//Stone D B, Runcorn S K. Flow and creep in the solar system: observations, modelling and theory. Dordrecht: Academic Publishers, 323-356.

Shakhova N, Semiletov I, Salyuk A, et al. 2010. Extensive methane venting to the atmosphere from sediments of the East Siberian Arctic Shelf. Science, 327(5970): 1246-1250, doi:10.1126/science.1182221.

Shipilov, E V, Murzin R R. 2002. Hydrocarbon deposits of western part of Russian shelf of Arctic: geology and systematic variations. Petrol Geol, 36(4): 325-347.

Shoji H, Minami H, Hachikubo A, et al. 2005. Hydrate-bearing structures in the Sea of Okhotsk. Eos Trans AGU, 86(2): 13-18, doi:10.1029/2005eo020001.

Solomon S, Qin D, Manning M, et al. 2007. Climate Change 2007: Synthesis Report. Contribution of Working Groups I, II, and III to the Fourth Assessment Report of the Intergovernmental Panel on Climate Change. Geneva, 104.

Susskind J, Barnet C D, Blaisdell J M. 2003. Retrieval of atmospheric and surface parameters from AIRS/AMSU/HSB data in the presence of clouds. IEEE Geosci Remote S, 41(2): 390-409, doi:10.1109/tgrs.2002.808236.

Susskind J, Blaisdell J, Iredell L. 2012. Significant advances in the AIRS Science Team Version-6 retrieval algorithm//Earth Observing Systems XVII. International Society for Optics and Photonics, 8510: 85100U, doi: 10.1117/12.929953.

Weber T, Wiseman N A, Kock A. 2019. Global ocean methane emissions dominated by shallow coastal waters. Nat Commun, 10: 4584, doi: 10.1038/s41467-019-12541-7.

Wunsch C, Heimbach P, Ponte R, et al. 2009. The global general circulation of the ocean estimated by the ECCO-consortium. Oceanog, 22(2): 88-103, doi:10.5670/oceanog.2009.41.

Xiong X Z, Barnet C, Maddy E, et al. 2008. Characterization and validation of methane products from the Atmospheric Infrared Sounder (AIRS). J Geophys Res, 113: G00A01, doi:10.1029/2007jg000500.

Yurganov L, Leifer I. 2016a. Estimates of methane emission rates from some Arctic and sub-Arctic areas, based on orbital interferometer IASI data. Curr Probl Remote Sens Earth From Space, 13(3): 173-183, doi:10.21046/2070-7401-2016-13-3-173-183 (in Russian with English abstract).

Yurganov L, Leifer I. 2016b. Abnormal concentrations of atmospheric methane over the Sea of Okhotsk during 2015/2016 winter. Curr Probl Remote Sens Earth From Space, 13(3): 231-234, doi:10.21046/2070-7401-2016-13-3-231-234 (in Russian with English abstract).

Yurganov L N, Leifer I, Myhre C L. 2016. Seasonal and interannual variability of atmospheric methane over Arctic Ocean from satellite data. Curr Probl Remote Sens Earth From Space, 13(2): 107-119, doi:10.21046/2070-7401-2016-13-2-107-119 (in Russian with English abstract).